

Novel method to extract the femtometer structure of strange baryons using the vacuum polarization effect

M. Ablikim¹, M. N. Achasov^{12,b}, P. Adlarson⁷², M. Albrecht⁴, R. Aliberti³³, A. Amoroso^{71A,71C}, M. R. An³⁷, Q. An^{68,55}, Y. Bai⁵⁴, O. Bakina³⁴, R. Baldini Ferroli^{27A}, I. Balossino^{28A}, Y. Ban^{44,g}, V. Batozskaya^{1,42}, D. Becker³³, K. Begzsuren³⁰, N. Berger³³, M. Bertani^{27A}, D. Bettoni^{28A}, F. Bianchi^{71A,71C}, E. Bianco^{71A,71C}, J. Bloms⁶⁵, A. Bortone^{71A,71C}, I. Boyko³⁴, R. A. Briere⁵, A. Brueggemann⁶⁵, H. Cai⁷³, X. Cai^{1,55}, A. Calcaterra^{27A}, G. F. Cao^{1,60}, N. Cao^{1,60}, S. A. Cetin^{59A}, J. F. Chang^{1,55}, W. L. Chang^{1,60}, G. R. Che⁴¹, G. Chelkov^{34,a}, C. Chen⁴¹, Chao Chen⁵², G. Chen¹, H. S. Chen^{1,60}, M. L. Chen^{1,55,60}, S. J. Chen⁴⁰, S. M. Chen⁵⁸, T. Chen^{1,60}, X. R. Chen^{29,60}, X. T. Chen^{1,60}, Y. B. Chen^{1,55}, Z. J. Chen^{24,h}, W. S. Cheng^{71C}, S. K. Choi⁵², X. Chu⁴¹, G. Cibinetto^{28A}, F. Cossio^{71C}, J. J. Cui⁴⁷, H. L. Dai^{1,55}, J. P. Dai⁷⁶, A. Dbeysi¹⁸, R. E. de Boer⁴, D. Dedovich³⁴, Z. Y. Deng¹, A. Denig³³, I. Denysenko³⁴, M. Destefanis^{71A,71C}, F. De Mori^{71A,71C}, Y. Ding³², Y. Ding³⁸, J. Dong^{1,55}, L. Y. Dong^{1,60}, M. Y. Dong^{1,55,60}, X. Dong⁷³, S. X. Du⁷⁸, Z. H. Duan⁴⁰, P. Egorov^{34,a}, Y. L. Fan⁷³, J. Fang^{1,55}, S. S. Fang^{1,60}, W. X. Fang¹, Y. Fang¹, R. Farinelli^{28A}, L. Fava^{71B,71C}, F. Feldbauer⁴, G. Felici^{27A}, C. Q. Feng^{68,55}, J. H. Feng⁵⁶, K. Fischer⁶⁶, M. Fritsch⁴, C. Fritsch⁶⁵, C. D. Fu¹, H. Gao⁶⁰, Y. N. Gao^{44,g}, Yang Gao^{68,55}, S. Garbolino^{71C}, I. Garzia^{28A,28B}, P. T. Ge⁷³, Z. W. Ge⁴⁰, C. Geng⁵⁶, E. M. Gersabeck⁶⁴, A. Gilman⁶⁶, K. Goetzen¹³, L. Gong³⁸, W. X. Gong^{1,55}, W. Gradl³³, M. Greco^{71A,71C}, L. M. Gu⁴⁰, M. H. Gu^{1,55}, Y. T. Gu¹⁵, C. Y. Guan^{1,60}, A. Q. Guo^{29,60}, L. B. Guo³⁹, R. P. Guo⁴⁶, Y. P. Guo^{11,f}, A. Guskov^{34,a}, W. Y. Han³⁷, X. Q. Hao¹⁹, F. A. Harris⁶², K. K. He⁵², K. L. He^{1,60}, F. H. Heinsius⁴, C. H. Heinz³³, Y. K. Heng^{1,55,60}, C. Herold⁵⁷, G. Y. Hou^{1,60}, Y. R. Hou⁶⁰, Z. L. Hou¹, H. M. Hu^{1,60}, J. F. Hu^{53,i}, T. Hu^{1,55,60}, Y. Hu¹, G. S. Huang^{68,55}, K. X. Huang⁵⁶, L. Q. Huang^{29,60}, X. T. Huang⁴⁷, Y. P. Huang¹, Z. Huang^{44,g}, T. Hussain⁷⁰, N. Hüskens^{26,33}, W. Imoehl²⁶, M. Irshad^{68,55}, J. Jackson²⁶, S. Jaeger⁴, S. Janchiv³⁰, E. Jang⁵², J. H. Jeong⁵², Q. Ji¹, Q. P. Ji¹⁹, X. B. Ji^{1,60}, X. L. Ji^{1,55}, Y. Y. Ji⁴⁷, Z. K. Jia^{68,55}, P. C. Jiang^{44,g}, S. S. Jiang³⁷, X. S. Jiang^{1,55,60}, Y. Jiang⁶⁰, J. B. Jiao⁴⁷, Z. Jiao²², S. Jin⁴⁰, Y. Jin⁶³, M. Q. Jing^{1,60}, T. Johansson⁷², S. Kabana³¹, N. Kalantar-Nayestanaki⁶¹, X. L. Kang⁹, X. S. Kang³⁸, R. Kappert⁶¹, M. Kavatsyuk⁶¹, B. C. Ke⁷⁸, I. K. Keshk⁴, A. Khoukaz⁶⁵, R. Kiuchi¹, R. Kliemt¹³, L. Koch³⁵, O. B. Kolcu^{59A}, B. Kopf⁴, M. Kuemmel⁴, M. Kuessner⁴, A. Kupsc^{42,72}, W. Kühn³⁵, J. J. Lane⁶⁴, J. S. Lange³⁵, P. Larin¹⁸, A. Lavanina²⁵, L. Lavezzi^{71A,71C}, T. T. Lei^{68,k}, Z. H. Lei^{68,55}, H. Leithoff⁴³, M. Lellmann³³, T. Lenz³³, C. Li⁴¹, C. H. Li³⁷, Cheng Li^{68,55}, D. M. Li⁷⁸, F. Li^{1,55}, G. Li¹, H. Li⁴⁹, H. Li^{68,55}, H. B. Li^{1,60}, H. J. Li¹⁹, H. N. Li^{53,i}, J. Q. Li⁴, J. S. Li⁵⁶, J. W. Li⁴⁷, Ke Li¹, L. J. Li^{1,60}, L. K. Li¹, Lei Li³, M. H. Li⁴¹, P. R. Li^{36,j,k}, S. X. Li¹¹, S. Y. Li⁵⁸, T. Li⁴⁷, W. D. Li^{1,60}, W. G. Li¹, X. H. Li^{68,55}, X. L. Li⁴⁷, Xiaoyu Li^{1,60}, Y. G. Li^{44,g}, Z. X. Li¹⁵, Z. Y. Li⁵⁶, C. Liang⁴⁰, H. Liang^{1,60}, H. Liang^{68,55}, H. Liang³², Y. F. Liang⁵¹, Y. T. Liang^{29,60}, G. R. Liao¹⁴, L. Z. Liao⁴⁷, J. Libby²⁵, A. Limphirat⁵⁷, C. X. Lin⁵⁶, D. X. Lin^{29,60}, T. Lin¹, B. J. Liu¹, C. Liu³², C. X. Liu¹, D. Liu^{18,68}, F. H. Liu⁵⁰, Fang Liu¹, Feng Liu⁶, G. M. Liu^{53,i}, H. Liu^{36,j,k}, H. B. Liu¹⁵, H. M. Liu^{1,60}, Huanhuan Liu¹, Huihui Liu²⁰, J. B. Liu^{68,55}, J. L. Liu⁶⁹, J. Y. Liu^{1,60}, K. Liu¹, K. Y. Liu³⁸, Ke Liu²¹, L. Liu^{68,55}, Lu Liu⁴¹, M. H. Liu^{11,f}, P. L. Liu¹, Q. Liu⁶⁰, S. B. Liu^{68,55}, T. Liu^{11,f}, W. K. Liu⁴¹, W. M. Liu^{68,55}, X. Liu^{36,j,k}, Y. Liu^{36,j,k}, Y. B. Liu⁴¹, Z. A. Liu^{1,55,60}, Z. Q. Liu⁴⁷, X. C. Lou^{1,55,60}, F. X. Lu⁵⁶, H. J. Lu²², J. G. Lu^{1,55}, X. L. Lu¹, Y. Lu⁷, Y. P. Lu^{1,55}, Z. H. Lu^{1,60}, C. L. Luo³⁹, M. X. Luo⁷⁷, T. Luo^{11,f}, X. L. Luo^{1,55}, X. R. Lyu⁶⁰, Y. F. Lyu⁴¹, F. C. Ma³⁸, H. L. Ma¹, L. L. Ma⁴⁷, M. M. Ma^{1,60}, Q. M. Ma¹, R. Q. Ma^{1,60}, R. T. Ma⁶⁰, X. Y. Ma^{1,55}, Y. Ma^{44,g}, F. E. Maas¹⁸, M. Maggiora^{71A,71C}, S. Maldaner⁴, S. Malde⁶⁶, Q. A. Malik⁷⁰, A. Mangoni^{27B}, Y. J. Mao^{44,g}, Z. P. Mao¹, S. Marcello^{71A,71C}, Z. X. Meng⁶³, J. G. Messchendorp^{13,61}, G. Mezzadri^{28A}, H. Miao^{1,60}, T. J. Min⁴⁰, R. E. Mitchell²⁶, X. H. Mo^{1,55,60}, N. Yu. Muchnoi^{12,b}, Y. Nefedov³⁴, F. Nerling^{18,d}, I. B. Nikolaev^{12,b}, Z. Ning^{1,55}, S. Nisar^{10,l}, Y. Niu⁴⁷, S. L. Olsen⁶⁰, Q. Ouyang^{1,55,60}, S. Pacetti^{27B,27C}, X. Pan⁵², Y. Pan⁵⁴, A. Pathak³², Y. P. Pei^{68,55}, M. Pelizaeus⁴, H. P. Peng^{68,55}, K. Peters^{13,d}, J. L. Ping³⁹, R. G. Ping^{1,60}, S. Plura³³, S. Pogodin³⁴, V. Prasad^{68,55}, F. Z. Qi¹, H. Qi^{68,55}, H. R. Qi⁵⁸, M. Qi⁴⁰, T. Y. Qi^{11,f}, S. Qian^{1,55}, W. B. Qian⁶⁰, Z. Qian⁵⁶, C. F. Qiao⁶⁰, J. J. Qin⁶⁹, L. Q. Qin¹⁴, X. P. Qin^{11,f}, X. S. Qin⁴⁷, Z. H. Qin^{1,55}, J. F. Qiu¹, S. Q. Qu⁵⁸, K. H. Rashid⁷⁰, C. F. Redmer³³, K. J. Ren³⁷, A. Rivetti^{71C}, V. Rodin⁶¹, M. Rolo^{71C}, G. Rong^{1,60}, Ch. Rosner¹⁸, S. N. Ruan⁴¹, A. Sarantsev^{34,c}, Y. Schelhaas³³, C. Schmier⁴, K. Schoenning⁷², M. Scodeggio^{28A,28B}, K. Y. Shan^{11,f}, W. Shan²³, X. Y. Shan^{68,55}, J. F. Shanguan⁵², L. G. Shao^{1,60}, M. Shao^{68,55}, C. P. Shen^{11,f}, H. F. Shen^{1,60}, W. H. Shen⁶⁰, X. Y. Shen^{1,60}, B. A. Shi⁶⁰, H. C. Shi^{68,55}, J. Y. Shi¹, Q. Q. Shi⁵², R. S. Shi^{1,60}, X. Shi^{1,55}, J. J. Song¹⁹, W. M. Song^{32,1}, Y. X. Song^{44,g}, S. Sosio^{71A,71C}, S. Spataro^{71A,71C}, F. Stieler³³, P. P. Su⁵², Y. J. Su⁶⁰, G. X. Sun¹, H. Sun⁶⁰, H. K. Sun¹, J. F. Sun¹⁹, L. Sun⁷³, S. S. Sun^{1,60}, T. Sun^{1,60}, W. Y. Sun³², Y. J. Sun^{68,55}, Y. Z. Sun¹, Z. T. Sun⁴⁷, Y. X. Tan^{68,55}, C. J. Tang⁵¹, G. Y. Tang¹, J. Tang⁵⁶, L. Y. Tao⁶⁹, Q. T. Tao^{24,h}, M. Tat⁶⁶, J. X. Teng^{68,55}, V. Thoren⁷², W. H. Tian⁴⁹, Y. Tian^{29,60}, I. Uman^{59B}, B. Wang¹, B. Wang^{68,55}, B. L. Wang⁶⁰, C. W. Wang⁴⁰, D. Y. Wang^{44,g}, F. Wang⁶⁹, H. J. Wang^{36,j,k}, H. P. Wang^{1,60}, K. Wang^{1,55}, L. L. Wang¹, M. Wang⁴⁷, M. Z. Wang^{44,g}, Meng Wang^{1,60}, S. Wang¹⁴, S. Wang^{11,f}, T. Wang^{11,f}, T. J. Wang⁴¹, W. Wang⁵⁶, W. H. Wang⁷³, W. P. Wang^{68,55}, X. Wang^{44,g}, X. F. Wang^{36,j,k}, X. L. Wang^{11,f},

Y. Wang⁵⁸, Y. D. Wang⁴³, Y. F. Wang^{1,55,60}, Y. H. Wang⁴⁵, Y. Q. Wang¹, Yaqian Wang^{17,1}, Z. Wang^{1,55}, Z. Y. Wang^{1,60}, Ziyi Wang⁶⁰, D. H. Wei¹⁴, F. Weidner⁶⁵, S. P. Wen¹, D. J. White⁶⁴, U. Wiedner⁴, G. Wilkinson⁶⁶, M. Wolke⁷², L. Wollenberg⁴, J. F. Wu^{1,60}, L. H. Wu¹, L. J. Wu^{1,60}, X. Wu^{11,f}, X. H. Wu³², Y. Wu⁶⁸, Y. J. Wu²⁹, Z. Wu^{1,55}, L. Xia^{68,55}, T. Xiang^{44,g}, D. Xiao^{36,j,k}, G. Y. Xiao⁴⁰, H. Xiao^{11,f}, S. Y. Xiao¹, Y. L. Xiao^{11,f}, Z. J. Xiao³⁹, C. Xie⁴⁰, X. H. Xie^{44,g}, Y. Xie⁴⁷, Y. G. Xie^{1,55}, Y. H. Xie⁶, Z. P. Xie^{68,55}, T. Y. Xing^{1,60}, C. F. Xu^{1,60}, C. J. Xu⁵⁶, G. F. Xu¹, H. Y. Xu⁶³, Q. J. Xu¹⁶, X. P. Xu⁵², Y. C. Xu⁷⁵, Z. P. Xu⁴⁰, F. Yan^{11,f}, L. Yan^{11,f}, W. B. Yan^{68,55}, W. C. Yan⁷⁸, H. J. Yang^{48,e}, H. L. Yang³², H. X. Yang¹, S. L. Yang^{1,60}, Tao Yang¹, Y. F. Yang⁴¹, Y. X. Yang^{1,60}, Yifan Yang^{1,60}, M. Ye^{1,55}, M. H. Ye⁸, J. H. Yin¹, Z. Y. You⁵⁶, B. X. Yu^{1,55,60}, C. X. Yu⁴¹, G. Yu^{1,60}, T. Yu⁶⁹, X. D. Yu^{44,g}, C. Z. Yuan^{1,60}, L. Yuan², S. C. Yuan¹, X. Q. Yuan¹, Y. Yuan^{1,60}, Z. Y. Yuan⁵⁶, C. X. Yue³⁷, A. A. Zafar⁷⁰, F. R. Zeng⁴⁷, X. Zeng⁶, Y. Zeng^{24,h}, X. Y. Zhai³², Y. H. Zhan⁵⁶, A. Q. Zhang^{1,60}, B. L. Zhang^{1,60}, B. X. Zhang¹, D. H. Zhang⁴¹, G. Y. Zhang¹⁹, H. Zhang⁶⁸, H. H. Zhang³², H. H. Zhang⁵⁶, H. Q. Zhang^{1,55,60}, H. Y. Zhang^{1,55}, J. L. Zhang⁷⁴, J. Q. Zhang³⁹, J. W. Zhang^{1,55,60}, J. X. Zhang^{36,j,k}, J. Y. Zhang¹, J. Z. Zhang^{1,60}, Jianyu Zhang^{1,60}, Jiawei Zhang^{1,60}, L. M. Zhang⁵⁸, L. Q. Zhang⁵⁶, Lei Zhang⁴⁰, P. Zhang¹, Q. Y. Zhang^{37,78}, Shuihan Zhang^{1,60}, Shulei Zhang^{24,h}, X. D. Zhang⁴³, X. M. Zhang¹, X. Y. Zhang⁴⁷, X. Y. Zhang⁵², Y. Zhang⁶⁶, Y. T. Zhang⁷⁸, Y. H. Zhang^{1,55}, Yan Zhang^{68,55}, Yao Zhang¹, Z. H. Zhang¹, Z. L. Zhang³², Z. Y. Zhang⁴¹, Z. Y. Zhang⁷³, G. Zhao¹, J. Zhao³⁷, J. Y. Zhao^{1,60}, J. Z. Zhao^{1,55}, Lei Zhao^{68,55}, Ling Zhao¹, M. G. Zhao⁴¹, S. J. Zhao⁷⁸, Y. B. Zhao^{1,55}, Y. X. Zhao^{29,60}, Z. G. Zhao^{68,55}, A. Zhemchugov^{34,a}, B. Zheng⁶⁹, J. P. Zheng^{1,55}, W. J. Zheng^{1,60}, Y. H. Zheng⁶⁰, B. Zhong³⁹, C. Zhong⁶⁹, X. Zhong⁵⁶, H. Zhou⁴⁷, L. P. Zhou^{1,60}, X. Zhou⁷³, X. K. Zhou⁶⁰, X. R. Zhou^{68,55}, X. Y. Zhou³⁷, Y. Z. Zhou^{11,f}, J. Zhu⁴¹, K. Zhu¹, K. J. Zhu^{1,55,60}, L. X. Zhu⁶⁰, S. H. Zhu⁶⁷, S. Q. Zhu⁴⁰, T. J. Zhu⁷⁴, W. J. Zhu^{11,f}, Y. C. Zhu^{68,55}, Z. A. Zhu^{1,60}, J. H. Zou¹, J. Zu^{68,55}

(BESIII Collaboration)

- ¹ *Institute of High Energy Physics, Beijing 100049, People's Republic of China*
² *Beihang University, Beijing 100191, People's Republic of China*
³ *Beijing Institute of Petrochemical Technology, Beijing 102617, People's Republic of China*
⁴ *Bochum Ruhr-University, D-44780 Bochum, Germany*
⁵ *Carnegie Mellon University, Pittsburgh, Pennsylvania 15213, USA*
⁶ *Central China Normal University, Wuhan 430079, People's Republic of China*
⁷ *Central South University, Changsha 410083, People's Republic of China*
⁸ *China Center of Advanced Science and Technology, Beijing 100190, People's Republic of China*
⁹ *China University of Geosciences, Wuhan 430074, People's Republic of China*
¹⁰ *COMSATS University Islamabad, Lahore Campus, Defence Road, Off Raiwind Road, 54000 Lahore, Pakistan*
¹¹ *Fudan University, Shanghai 200433, People's Republic of China*
¹² *G.I. Budker Institute of Nuclear Physics SB RAS (BINP), Novosibirsk 630090, Russia*
¹³ *GSI Helmholtzcentre for Heavy Ion Research GmbH, D-64291 Darmstadt, Germany*
¹⁴ *Guangxi Normal University, Guilin 541004, People's Republic of China*
¹⁵ *Guangxi University, Nanning 530004, People's Republic of China*
¹⁶ *Hangzhou Normal University, Hangzhou 310036, People's Republic of China*
¹⁷ *Hebei University, Baoding 071002, People's Republic of China*
¹⁸ *Helmholtz Institute Mainz, Staudinger Weg 18, D-55099 Mainz, Germany*
¹⁹ *Henan Normal University, Xinxiang 453007, People's Republic of China*
²⁰ *Henan University of Science and Technology, Luoyang 471003, People's Republic of China*
²¹ *Henan University of Technology, Zhengzhou 450001, People's Republic of China*
²² *Huangshan College, Huangshan 245000, People's Republic of China*
²³ *Hunan Normal University, Changsha 410081, People's Republic of China*
²⁴ *Hunan University, Changsha 410082, People's Republic of China*
²⁵ *Indian Institute of Technology Madras, Chennai 600036, India*
²⁶ *Indiana University, Bloomington, Indiana 47405, USA*
²⁷ *INFN Laboratori Nazionali di Frascati, (A)INFN Laboratori Nazionali di Frascati, I-00044, Frascati, Italy; (B)INFN Sezione di Perugia, I-06100, Perugia, Italy; (C)University of Perugia, I-06100, Perugia, Italy*
²⁸ *INFN Sezione di Ferrara, (A)INFN Sezione di Ferrara, I-44122, Ferrara, Italy; (B)University of Ferrara, I-44122, Ferrara, Italy*
²⁹ *Institute of Modern Physics, Lanzhou 730000, People's Republic of China*
³⁰ *Institute of Physics and Technology, Peace Avenue 54B, Ulaanbaatar 13330, Mongolia*
³¹ *Instituto de Alta Investigación, Universidad de Tarapacá, Casilla 7D, Arica, Chile*
³² *Jilin University, Changchun 130012, People's Republic of China*

- ³³ Johannes Gutenberg University of Mainz, Johann-Joachim-Becher-Weg 45, D-55099 Mainz, Germany
- ³⁴ Joint Institute for Nuclear Research, 141980 Dubna, Moscow region, Russia
- ³⁵ Justus-Liebig-Universitaet Giessen, II. Physikalisches Institut, Heinrich-Buff-Ring 16, D-35392 Giessen, Germany
- ³⁶ Lanzhou University, Lanzhou 730000, People's Republic of China
- ³⁷ Liaoning Normal University, Dalian 116029, People's Republic of China
- ³⁸ Liaoning University, Shenyang 110036, People's Republic of China
- ³⁹ Nanjing Normal University, Nanjing 210023, People's Republic of China
- ⁴⁰ Nanjing University, Nanjing 210093, People's Republic of China
- ⁴¹ Nankai University, Tianjin 300071, People's Republic of China
- ⁴² National Centre for Nuclear Research, Warsaw 02-093, Poland
- ⁴³ North China Electric Power University, Beijing 102206, People's Republic of China
- ⁴⁴ Peking University, Beijing 100871, People's Republic of China
- ⁴⁵ Qufu Normal University, Qufu 273165, People's Republic of China
- ⁴⁶ Shandong Normal University, Jinan 250014, People's Republic of China
- ⁴⁷ Shandong University, Jinan 250100, People's Republic of China
- ⁴⁸ Shanghai Jiao Tong University, Shanghai 200240, People's Republic of China
- ⁴⁹ Shanxi Normal University, Linfen 041004, People's Republic of China
- ⁵⁰ Shanxi University, Taiyuan 030006, People's Republic of China
- ⁵¹ Sichuan University, Chengdu 610064, People's Republic of China
- ⁵² Soochow University, Suzhou 215006, People's Republic of China
- ⁵³ South China Normal University, Guangzhou 510006, People's Republic of China
- ⁵⁴ Southeast University, Nanjing 211100, People's Republic of China
- ⁵⁵ State Key Laboratory of Particle Detection and Electronics, Beijing 100049, Hefei 230026, People's Republic of China
- ⁵⁶ Sun Yat-Sen University, Guangzhou 510275, People's Republic of China
- ⁵⁷ Suranaree University of Technology, University Avenue 111, Nakhon Ratchasima 30000, Thailand
- ⁵⁸ Tsinghua University, Beijing 100084, People's Republic of China
- ⁵⁹ Turkish Accelerator Center Particle Factory Group, (A)Istinye University, 34010, Istanbul, Turkey; (B)Near East University, Nicosia, North Cyprus, Mersin 10, Turkey
- ⁶⁰ University of Chinese Academy of Sciences, Beijing 100049, People's Republic of China
- ⁶¹ University of Groningen, NL-9747 AA Groningen, The Netherlands
- ⁶² University of Hawaii, Honolulu, Hawaii 96822, USA
- ⁶³ University of Jinan, Jinan 250022, People's Republic of China
- ⁶⁴ University of Manchester, Oxford Road, Manchester, M13 9PL, United Kingdom
- ⁶⁵ University of Muenster, Wilhelm-Klemm-Strasse 9, 48149 Muenster, Germany
- ⁶⁶ University of Oxford, Keble Road, Oxford OX13RH, United Kingdom
- ⁶⁷ University of Science and Technology Liaoning, Anshan 114051, People's Republic of China
- ⁶⁸ University of Science and Technology of China, Hefei 230026, People's Republic of China
- ⁶⁹ University of South China, Hengyang 421001, People's Republic of China
- ⁷⁰ University of the Punjab, Lahore-54590, Pakistan
- ⁷¹ University of Turin and INFN, (A)University of Turin, I-10125, Turin, Italy; (B)University of Eastern Piedmont, I-15121, Alessandria, Italy; (C)INFN, I-10125, Turin, Italy
- ⁷² Uppsala University, Box 516, SE-75120 Uppsala, Sweden
- ⁷³ Wuhan University, Wuhan 430072, People's Republic of China
- ⁷⁴ Xinyang Normal University, Xinyang 464000, People's Republic of China
- ⁷⁵ Yantai University, Yantai 264005, People's Republic of China
- ⁷⁶ Yunnan University, Kunming 650500, People's Republic of China
- ⁷⁷ Zhejiang University, Hangzhou 310027, People's Republic of China
- ⁷⁸ Zhengzhou University, Zhengzhou 450001, People's Republic of China
- ^a Also at the Moscow Institute of Physics and Technology, Moscow 141700, Russia
- ^b Also at the Novosibirsk State University, Novosibirsk, 630090, Russia
- ^c Also at the NRC "Kurchatov Institute", PNPI, 188300, Gatchina, Russia
- ^d Also at Goethe University Frankfurt, 60323 Frankfurt am Main, Germany
- ^e Also at Key Laboratory for Particle Physics, Astrophysics and Cosmology, Ministry of Education; Shanghai Key Laboratory for Particle Physics and Cosmology; Institute of Nuclear and Particle Physics, Shanghai 200240, People's Republic of China

^f Also at Key Laboratory of Nuclear Physics and Ion-beam Application (MOE) and Institute of Modern Physics, Fudan University, Shanghai 200443, People's Republic of China

^g Also at State Key Laboratory of Nuclear Physics and Technology, Peking University, Beijing 100871, People's Republic of China

^h Also at School of Physics and Electronics, Hunan University, Changsha 410082, China

ⁱ Also at Guangdong Provincial Key Laboratory of Nuclear Science, Institute of Quantum Matter, South China Normal University, Guangzhou 510006, China

^j Also at Frontiers Science Center for Rare Isotopes, Lanzhou University, Lanzhou 730000, People's Republic of China

^k Also at Lanzhou Center for Theoretical Physics, Lanzhou University, Lanzhou 730000, People's Republic of China

^l Also at the Department of Mathematical Sciences, IBA, Karachi, Pakistan

(Dated: September 11, 2023)

One of the fundamental goals of particle physics is to gain microscopic understanding of the strong interaction. Electromagnetic form factors quantify the structure of hadrons in terms of charge and magnetization distributions. While the nucleon structure has been investigated extensively, data on hyperons is still scarce. It has recently been demonstrated that electron-positron annihilations into hyperon-antihyperon pairs provide a powerful tools to investigate their inner structure. We present a novel method useful for hyperon-antihyperon pairs of different types which exploits the cross section enhancement due to the vacuum polarization effect at the J/ψ resonance. Using the 10 billion J/ψ events collected with the BESIII detector, this allows a thorough determination of the hyperon structure. The result is essentially a precise snapshot of a $\bar{\Lambda}\Sigma^0$ ($\Lambda\bar{\Sigma}^0$) pair in the making, encoded in the form factor ratio and the phase. Their values are measured to be $R = 0.860 \pm 0.029(\text{stat.}) \pm 0.010(\text{syst.})$, $\Delta\Phi_1 = (1.011 \pm 0.094(\text{stat.}) \pm 0.010(\text{syst.}))$ rad for $\bar{\Lambda}\Sigma^0$ and $\Delta\Phi_2 = (2.128 \pm 0.094(\text{stat.}) \pm 0.010(\text{syst.}))$ rad for $\Lambda\bar{\Sigma}^0$, respectively. Furthermore, charge-parity (CP) breaking is investigated for the first time in this reaction and found to be consistent with CP symmetry.

I. INTRODUCTION

One distinctive feature of the strong nuclear interaction and a prerequisite for our existence is the confinement of nearly massless quarks into stable and massive hadrons such as protons or neutrons that constitute the matter we are made of. A coherent understanding of the dynamics of the strong interaction, however, remains one of the most intriguing puzzles of physics. The main challenge is the very nature of confinement: the quarks and gluons cannot be observed as bare particles, but are “dressed” by the strong interaction into quasi-particles, or constituent quarks, that form the bound systems we know as hadrons. The distribution and motion of quarks inside hadrons is quantified in terms of, e.g., electromagnetic form factors which offer an empirical tool to study the strong dynamics. The proton, as the most stable composite particle we know (with a lifetime much longer than the age of the Universe), offers an excellent testing ground for the strong interaction. The space-like form factors of the proton have been subject of rigorous studies since 1956, when Hofstadter introduced the electron scattering techniques [1]. To this day, new and surprising features are being discovered [2–

4] and debated [5–7].

A common strategy to achieve a deeper understanding of these features is to investigate the impact of introducing heavy and unstable quarks into the bound system. The lightest siblings of the proton are the Λ and the Σ^0 hyperons, both consisting of an up-quark (u), a down-quark (d) and a heavy and unstable strange-quark (s), in contrast to the proton with a uud structure of only light quarks. Since hyperons are unstable, they cannot be studied with conventional electron scattering techniques. Instead, their timelike form factors can be accessed in electron-positron annihilations with the subsequent production of a hyperon-antihyperon pair, and in hyperon Dalitz decays. The timelike form factors can be seen as “snapshots” of the time evolution of a hyperon-antihyperon pair, carrying information about the space-like structure. The space-like and timelike regions are related via dispersion relations. In recent years, the BESIII collaboration has performed pioneering studies of hyperon form factors [8–21]. In particular, the self-analyzing hyperon decays can be used to measure the hyperon polarization, thereby completely determining the form factors of the Λ hyperon [22]. However, timelike form

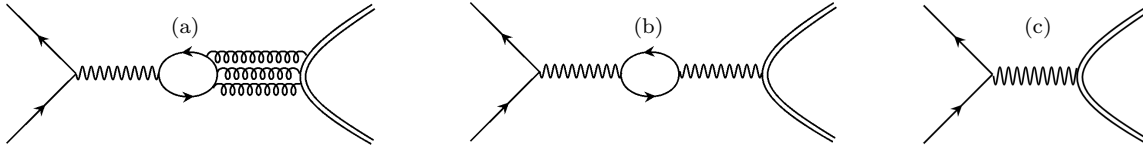


FIG. 1. The Feynman diagrams for $e^+e^- \rightarrow \text{hadrons}$ in the vicinity of the J/ψ . (a) strong process with intermediate J/ψ mediated by gluons, (b) electromagnetic process through the vacuum polarization of one virtual photon to a J/ψ , (c) continuum process without the J/ψ intermediate state but only one virtual photon.

factors need to be studied in processes where a one-photon exchange is the dominating process, as shown in Fig. 1(c). For a hyperon-antihyperon pair of the same type, e.g. $\Lambda\bar{\Lambda}$, this means that the electron-positron annihilation must occur at an energy far from any vector meson resonances that can decay strongly into a hyperon-antihyperon pair. For a pair where the hyperon and the antihyperon are of different type, e.g. $\Lambda\bar{\Sigma}^0$ or $\bar{\Lambda}\Sigma^0$, Ref. [23] proposed the method of comparing the modulus values of the same electromagnetic coupling extracted from the branching ratio of $J/\psi \rightarrow \bar{\Lambda}\Sigma^0 + c.c.$ and the cross section of the reaction $e^+e^- \rightarrow \bar{\Lambda}\Sigma^0 + c.c.$ at the J/ψ mass, along with the experimental values of the scaled cross section from BESIII and BaBar data. This suggests that the diagram in Fig. 1(a) is absent since the process is isospin violating. Hence, $e^+e^- \rightarrow J/\psi \rightarrow \bar{\Lambda}\Sigma^0$ must be a purely electromagnetic process [23], as depicted in Fig. 1(b), which has the same final production vertex as Fig. 1(c). Accordingly, the electric and magnetic form factors of Fig. 1(c) can be extracted from Fig. 1(b) by correcting for the well known vacuum polarization. This demonstrates that the transition form factor of $\Lambda\bar{\Sigma}^0$ is accessible both in the low-energy region via Dalitz decay and in the high-energy region through e^+e^- annihilations [24], which means we can measure the structure over a much broader energy range than other hyperons. By exploiting quantum entangled pairs of Σ^0 ($\bar{\Sigma}^0$) and $\bar{\Lambda}$ (Λ), where Σ^0 ($\bar{\Sigma}^0$) decays sequentially via intermediate $\bar{\Lambda}$ (Λ) hyperons, we investigate the reaction $e^+e^- \rightarrow J/\psi \rightarrow \bar{\Lambda}\Sigma^0$. We compare this isospin symmetry breaking and therefore purely electromagnetic transition to the isospin conserving $J/\psi \rightarrow Y\bar{Y}$ decay, which is an interplay of strong and electromagnetic interactions. With the hadronic vacuum polarization resulting in a significantly enhanced signal, we probe the same vertex as the one-photon exchange process and attain the structure at the J/ψ resonance. At

present, the available $(10087 \pm 44) \times 10^6$ J/ψ events produced in e^+e^- annihilations [25] at BESIII, almost one order of magnitude larger than the data sample used in the previous measurement [11], offer us a great opportunity to investigate the form factors with the polarized entangled $\Lambda\bar{\Sigma}^0$ pairs. The inclusion of charge-conjugate processes is implied hereafter unless explicitly mentioned otherwise.

II. ANALYSIS

The BESIII detector [26] records symmetric e^+e^- collisions provided by the BEPCII storage ring [27], which operates with a peak luminosity of $10^{33} \text{ cm}^{-2}\text{s}^{-1}$ in the centre-of-mass energy (\sqrt{s}) range from 2.0 to 4.95 GeV. In this cylindrical system, tracks of charged particles in the detector are reconstructed from track-induced signals and the momenta are determined from the track curvature in the main drift chamber (MDC). The flight time of charged particles is recorded by a plastic scintillator time-of-flight system (TOF). Showers from photon clusters are reconstructed and energy deposits are measured in the electromagnetic calorimeter (EMC). The signal of $e^+e^- \rightarrow J/\psi \rightarrow \bar{\Lambda}(\rightarrow \bar{p}\pi^+)\Sigma^0(\rightarrow \gamma\Lambda \rightarrow \gamma p\pi^-)$ is extracted from $(10087 \pm 44) \times 10^6$ J/ψ events [25] at $\sqrt{s} = 3.097$ GeV. The Λ ($\bar{\Lambda}$) is reconstructed using $p\pi^-$ ($\bar{p}\pi^+$) decays and Σ^0 from $\gamma\Lambda$ decays. The specific requirements of event reconstruction and selection criteria are described in Appendix A 2 and A 3. The resulting signals of $\bar{\Lambda}(\Lambda)$ and $\Sigma^0(\bar{\Sigma}^0)$ are clearly observed, as shown in Figs. 2 and 3. The possible background events are investigated with an inclusive Monte Carlo (MC) sample generated with all known J/ψ decays. To estimate the number of background events coming directly from the continuum light hadron (QED) process, the same analysis is performed on the data sample at $\sqrt{s} = 3.080$ GeV,

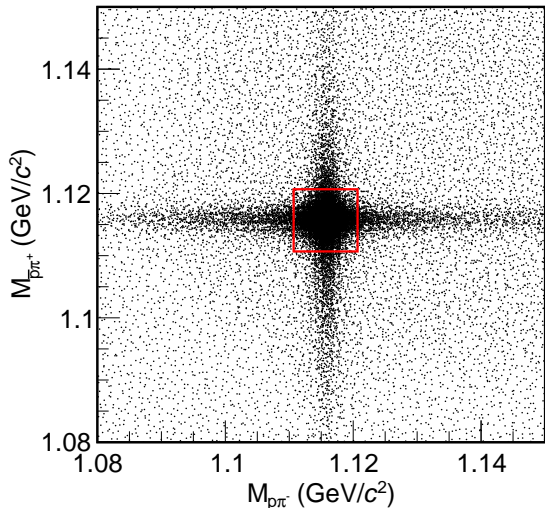


FIG. 2. Distribution of $M_{p\pi^-}$ versus $M_{p\pi^+}$ of the accepted candidates from data. The red box denotes the signal region. The clusters of Λ and $\bar{\Lambda}$ are clearly observed.

corresponding to an integrated luminosity of 166.3 pb^{-1} [25]. With an extended unbinned maximum likelihood fit to the $\gamma\Lambda$ ($\gamma\bar{\Lambda}$) invariant mass distribution shown in Fig. 4, the final signal yields are determined to be 26260 ± 181 and the QED background are 39 ± 7 . The details of background analysis and fit are described in Appendix A 4.

Based on the studies of $e^+e^- \rightarrow \mu^+\mu^-$ and $\eta\pi^+\pi^-$ in Ref. [28], the relative phase between the hadronic vacuum (Fig. 1(b)) and the continuum (Fig. 1(c)) processes is zero in case of a purely electromagnetic decay, and it has a line shape similar to the cross section of the purely electromagnetic process. Consequently, the ratio of the cross section at the J/ψ peak to that at any specific energy is the same for different purely electromagnetic processes as illustrated by both $e^+e^- \rightarrow \mu^+\mu^-$ and $\eta\pi^+\pi^-$. With the measured cross sections in Ref. [28], the corresponding ratios of these two processes are calculated to be 24.20 ± 0.81 and 28.81 ± 8.52 , respectively, both in good agreement with each other. Here, the uncertainties are statistical only since the systematic uncertainties cancel in the calculation of the ratio. We also performed the measurement of the cross sections of $e^+e^- \rightarrow \bar{\Lambda}\Sigma^0 + c.c.$ at the J/ψ peak and at 3.08 GeV, determining the corresponding ratio to be 33.72 ± 6.06 . This value is consistent with those from the above processes with-

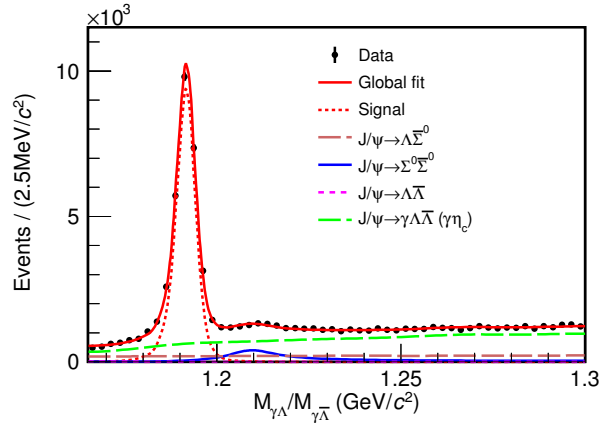


FIG. 3. Fit to the $M_{\gamma\Lambda}/M_{\gamma\bar{\Lambda}}$ distribution of the accepted candidates from J/ψ data. The black points with error bars are data, the red curve is the global fit, the red dotted curve is the $\Sigma^0/\bar{\Sigma}^0$ signal, the brown long-dashed curve shows the background from the conjugate channel, the blue curve is from $J/\psi \rightarrow \Sigma^0\bar{\Sigma}^0$, the pink dotted curve is from $J/\psi \rightarrow \Lambda\bar{\Lambda}$ and the green long-dashed curve is from $J/\psi \rightarrow \gamma\Lambda\bar{\Lambda}(\gamma\eta_c)$.

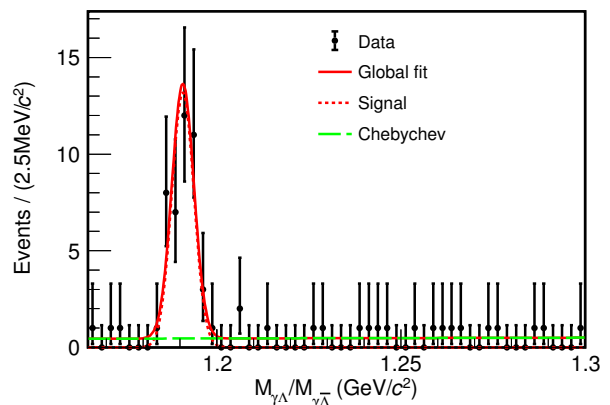


FIG. 4. Fit to the $M_{\gamma\Lambda}/M_{\gamma\bar{\Lambda}}$ distribution from the QED background. The black points with error bars are data, the red curve is the global fit, the red dotted curve is the signal shape described by a Breit-Wigner shape convolved with a Gaussian function and the green long-dashed curve is from the background described with a first-order Chebychev function.

in the uncertainties, thus providing further evidence for $J/\psi \rightarrow \bar{\Lambda}\Sigma^0 + c.c.$ as a purely electromagnetic decay, which implies a novel way to extract the electromagnetic form factor with the hadronic vacuum polarization at the J/ψ peak.

Since the imaginary part of form factors is non-zero at centre-of-mass energies above the two-pion threshold [29, 30], the relative phase $\Delta\Phi$ between the electric and magnetic form factors, G_E and G_M , is expected to be non-zero. In case of $e^+e^- \rightarrow J/\psi \rightarrow \bar{\Lambda}\Sigma^0$, a non-vanishing $\Delta\Phi$ also demonstrates the polarization of Λ and Σ^0 in the direction perpendicular to the production plane. Since the electron mass is negligible in comparison to the J/ψ mass, the initial electron and positron helicities have to be opposite. This implies that the angular distribution and polarization can be described uniquely by only two quantities, the relative phase $\Delta\Phi = \arg(G_E/G_M)$ and the angular distribution parameter $\alpha = \frac{s-4M_Y^2 R^2}{s+4M_Y^2 R^2}$ [31], where $R = |\frac{G_E}{G_M}|$ and M_Y is the mass of the final hyperon. For $\bar{\Lambda}\Sigma^0$ ($\Lambda\Sigma^0$), M_Y is replaced by $(M_{\Sigma^0} + M_\Lambda)/2$ [32]. The probability of extracting the form factors in the production and cascade decays of $e^+e^- \rightarrow J/\psi \rightarrow \bar{\Lambda}(\rightarrow \bar{p}\pi^+) \Sigma^0(\rightarrow \gamma\Lambda \rightarrow \gamma p\pi^-)$ is described by the six kinematic variables as described in Appendix A 6, expressed as the helicity angles $\xi = (\theta, \theta_\Lambda, \phi_\Lambda, \theta_p, \theta_{\bar{p}}, \phi_{\bar{p}})$ shown in Fig. 5.

Here, we denote the angular distribution parameter, the relative phase and decay asymmetries for $\Sigma^0 \rightarrow \gamma\Lambda$, $\Lambda \rightarrow p\pi^-$, and $\bar{\Lambda} \rightarrow \bar{p}\pi^+$ as $\alpha_{J/\psi}$, $\Delta\Phi$, α_γ , α_Λ , and $\alpha_{\bar{\Lambda}}$, respectively. Subsequently, to extract the form factors, the helicity analysis is performed for $J/\psi \rightarrow \bar{\Lambda}\Sigma^0 + c.c.$ based on the angular distribution as described in detail in Appendix A 6. Although $e^+e^- \rightarrow J/\psi \rightarrow \Lambda\Sigma^0$ and $e^+e^- \rightarrow J/\psi \rightarrow \bar{\Lambda}\Sigma^0$ are two independent reactions, their helicity amplitudes are simply related before and after charge-conjugate and parity transformation. As a result, the relative phases $\Delta\Phi$ of these two decays are expected to satisfy $\Delta\Phi_1 + \Delta\Phi_2 = \pi$, where $\Delta\Phi_1$ and $\Delta\Phi_2$ denote the relative phases of timelike electric and magnetic form factors for $e^+e^- \rightarrow J/\psi \rightarrow \bar{\Lambda}\Sigma^0$ and $e^+e^- \rightarrow J/\psi \rightarrow \Lambda\Sigma^0$, respectively. Therefore, the simultaneous measurement of $\bar{\Lambda}\Sigma^0$ and $\Lambda\Sigma^0$ offers the possibility to explore CP violation by evaluating $\Delta\Phi_{CP} = |\pi - (\Delta\Phi_1 + \Delta\Phi_2)|$, which is required to be zero from CP invariance.

In the Σ mass region, a combined helicity analysis is performed for $J/\psi \rightarrow \bar{\Lambda}\Sigma^0$ and $J/\psi \rightarrow \Lambda\Sigma^0$ and the parameters α_Λ and $\alpha_{\bar{\Lambda}}$ are fixed to be $\alpha_\Lambda = 0.7519$ and $\alpha_{\bar{\Lambda}} = -0.7559$ [33] from previous high-precision

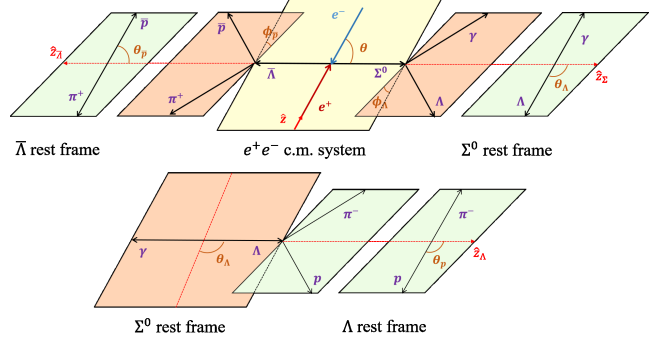


FIG. 5. Definition of the helicity angles for $J/\psi \rightarrow \bar{\Lambda}(\rightarrow \bar{p}\pi^+) \Sigma^0(\rightarrow \gamma\Lambda \rightarrow \gamma p\pi^-)$. The angles $\theta, \theta_\Lambda, \theta_p, \theta_{\bar{p}}$ are the polar helicity angles of the Σ^0, Λ, p and \bar{p} in the e^+e^- center-of-mass system, Σ^0 rest frame, Λ rest frame and $\bar{\Lambda}$ rest frame, respectively. The angles between different decay or production planes, ϕ_Λ and $\phi_{\bar{p}}$, are the azimuthal helicity angles of the Λ and \bar{p} in the Σ^0 rest frame and Λ rest frame, respectively. In the e^+e^- center-of-mass system, the \hat{z} is along the e^+ momentum direction, and the \hat{z}_Σ is along the Σ^0 outgoing direction. In the Σ^0 rest frame, the polar axis is \hat{z}_Σ , \hat{y}_Σ is along $\hat{z} \times \hat{z}_\Sigma$ and \hat{z}_Λ is along the Λ outgoing direction. In the Λ rest frame, the polar axis is \hat{z}_Λ , and \hat{y}_Λ is along $\hat{z}_\Sigma \times \hat{z}_\Lambda$. In the $\bar{\Lambda}$ rest frame, the polar axis is $\hat{z}_{\bar{\Lambda}}$, and $\hat{y}_{\bar{\Lambda}}$ is along $\hat{z} \times \hat{z}_{\bar{\Lambda}}$.

measurements of $J/\psi \rightarrow \Lambda\bar{\Lambda}$. Using the average magnitude for both has a negligible effect on fit results. Due to the electromagnetic part of the decay chain, $\Sigma^0 \rightarrow \gamma\Lambda$, where the photon polarization is not measured [34], the α_γ is presumed to be 0. The free parameters, including $\alpha_{J/\psi}$ and the relative phase $\Delta\Phi_1$ ($\Delta\Phi_2$) for $e^+e^- \rightarrow J/\psi \rightarrow \bar{\Lambda}\Sigma^0$ ($\Lambda\Sigma^0$), are optimized with an unbinned maximum likelihood fit defined in Appendix A 7. These parameters are measured by incorporating the transverse polarization of Σ^0 ($\bar{\Sigma}^0$) in the joint angular distribution. The global fit is represented by the multidimensional angular distributions shown in Figs. 6 and 7 with a specific fitting technique as well as systematic uncertainties described in Appendix A 8.

III. RESULTS

From the global fit, a prominent polarization and strong correlation of the relative phase between the two processes are observed, characterized by P_y elucidating the spin transverse polarization and C_{xz} repre-

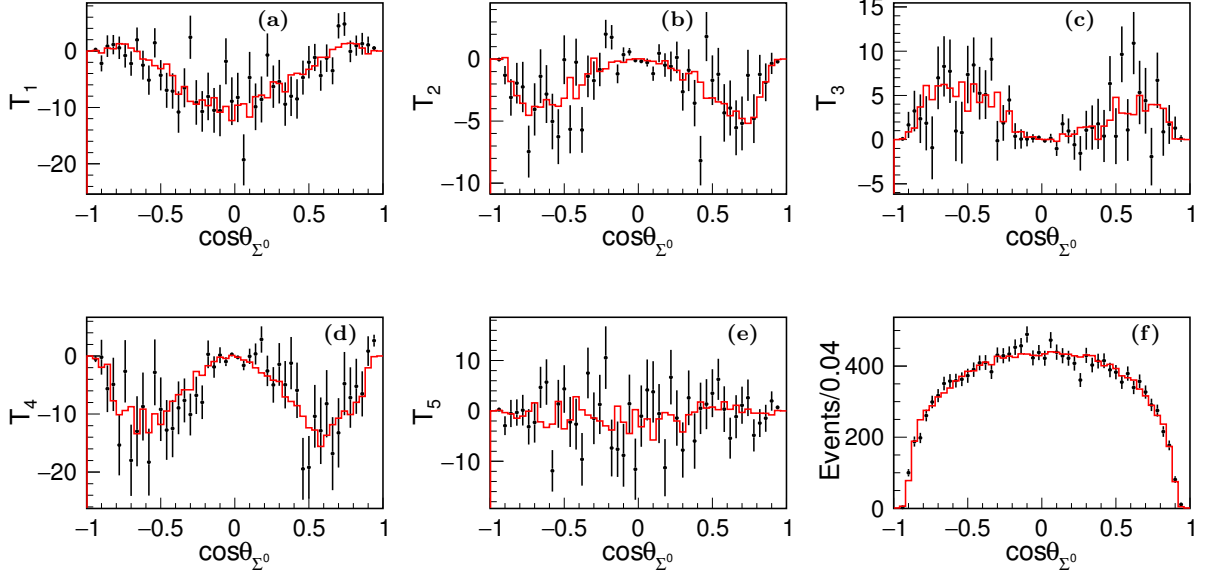


FIG. 6. Fit results compared with data of $e^+e^- \rightarrow J/\psi \rightarrow \bar{\Lambda}(\rightarrow \bar{p}\pi^+) \Sigma^0(\rightarrow \gamma\Lambda)$ process. (a)-(e) are the moments T_1 - T_5 respectively and (f) is the Σ^0 angular distribution. The black points with error bars are data and the red curve is the global fit.

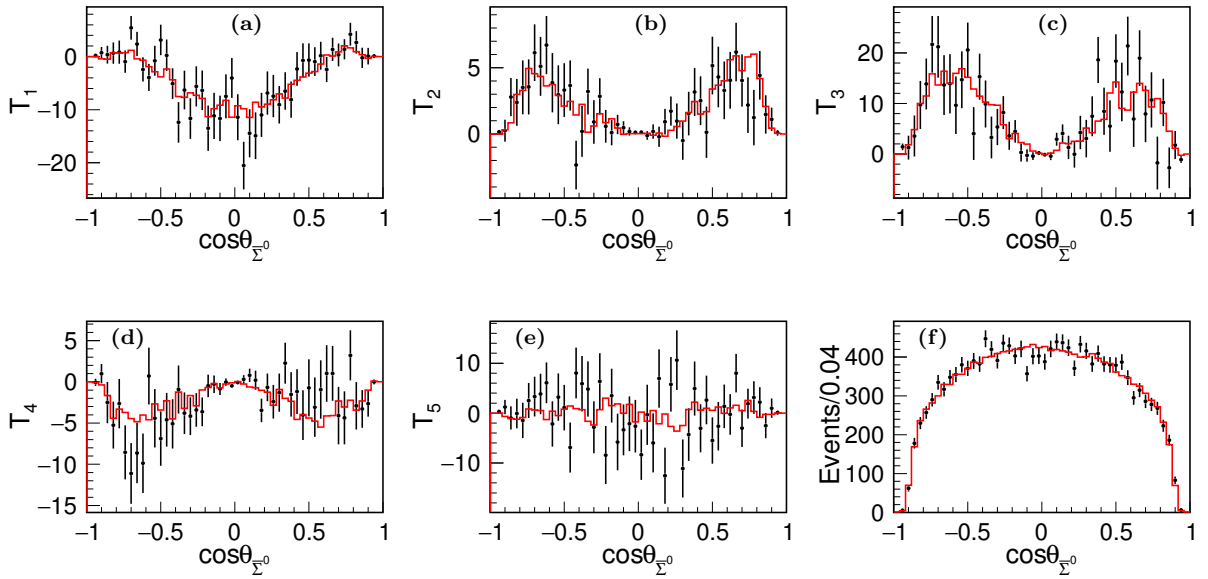


FIG. 7. Fit results compared with data of $e^+e^- \rightarrow J/\psi \rightarrow \Lambda(\rightarrow p\pi^-) \bar{\Sigma}^0(\rightarrow \gamma\bar{\Lambda})$ process. (a)-(e) is the moments T_1 - T_5 respectively and (f) is the $\bar{\Sigma}^0$ angular distribution. The black points with error bars are data and the red curve is the global fit

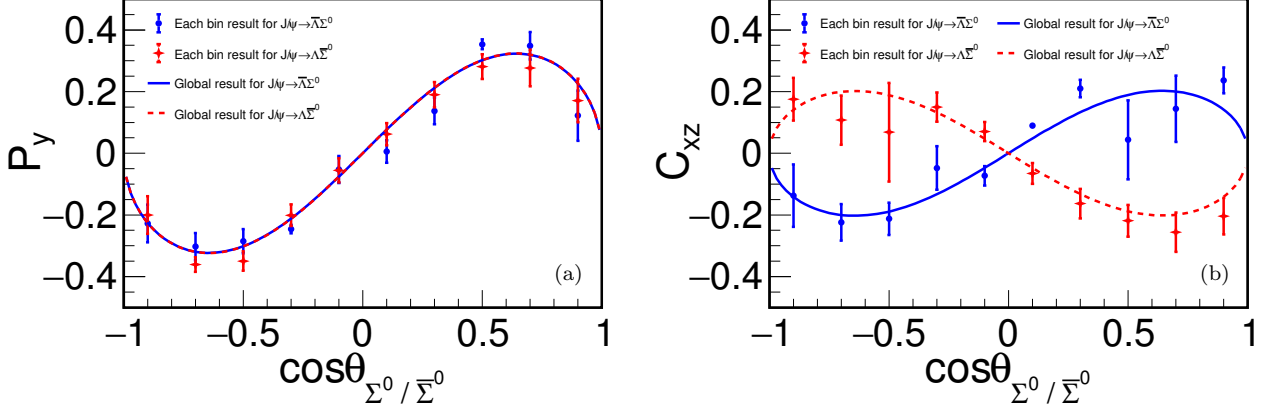


FIG. 8. Polarization P_y and spin correlations C_{xz} in $e^+e^- \rightarrow J/\psi \rightarrow \bar{\Lambda}\Sigma^0(\Lambda\bar{\Sigma}^0)$. The points with error bars, blue solid dot for $J/\psi \rightarrow \bar{\Lambda}\Sigma^0$ and red open double diamond for $J/\psi \rightarrow \Lambda\bar{\Sigma}^0$, are extracted in each $\cos\theta_{\Sigma^0}(\cos\theta_{\bar{\Sigma}^0})$ bin, and the blue solid curves denote the global expected dependence on $\cos\theta_{\Sigma^0}(\cos\theta_{\bar{\Sigma}^0}$ for the red dotted curve).

senting the particular relationship between $\Delta\Phi_1$ and $\Delta\Phi_2$. Their strong dependence on the Σ^0 ($\bar{\Sigma}^0$) direction angle θ , defined in Appendix A 6, is seen in Fig. 8. To illustrate the fit quality, the fit results in each $\cos\theta_{\Sigma^0}/\bar{\Sigma}^0$ bin are also shown using points with error bars in Fig. 8. Apart from the difference caused by the fluctuations from the complex background channels, the points of each bin are consistent with the globally fitted curves.

The fit yields $\alpha_{J/\psi} = 0.418 \pm 0.028(\text{stat.}) \pm 0.010(\text{syst.})$, $\Delta\Phi_1 = (1.011 \pm 0.094(\text{stat.}) \pm 0.010(\text{syst.}))$ rad, and $\Delta\Phi_2 = (2.128 \pm 0.094(\text{stat.}) \pm 0.010(\text{syst.}))$ rad. The ratio $R = |\frac{G_E}{G_M}| = \frac{\sqrt{s}}{2M_Y} \sqrt{\frac{1-\alpha}{1+\alpha}}$ is determined to be $0.860 \pm 0.029(\text{stat.}) \pm 0.010(\text{syst.})$, giving the ratio and relative phase of the electric and magnetic form factors G_E and G_M for $e^+e^- \rightarrow J/\psi \rightarrow \bar{\Lambda}\Sigma^0$ ($\Lambda\bar{\Sigma}^0$) at $\sqrt{s} = 3.097$ GeV, with clear transverse spin polarizations of the Λ and $\bar{\Sigma}^0$ observed. The sum of these two relative phases, $\Delta\Phi_1 + \Delta\Phi_2 = (3.139 \pm 0.133(\text{stat.}) \pm 0.014(\text{syst.}))$ rad, is in good agreement with the expected value of π . $\Delta\Phi_{\text{CP}} = |\pi - (\Delta\Phi_1 + \Delta\Phi_2)|$ is calculated to be $0.003 \pm 0.133(\text{stat.}) \pm 0.014(\text{syst.})$, which is consistent with zero and indicates no evident direct CP violation in the decays of $J/\psi \rightarrow \bar{\Lambda}\Sigma^0$ and $J/\psi \rightarrow \Lambda\bar{\Sigma}^0$. It is the first time that the timelike structure for $e^+e^- \rightarrow \bar{\Lambda}\Sigma^0 + c.c.$ is extracted at $\sqrt{s} = 3.097$ GeV with high precision by using the hadronic vacuum polarization

enhancement at the J/ψ . In addition, unlike e^+e^- annihilation into hyperon anti-hyperon pairs, Λ and $\bar{\Sigma}^0$ are not charge conjugates of each other which enables us to explore direct CP violation by comparison of polarizations from both $e^+e^- \rightarrow J/\psi \rightarrow \Lambda\bar{\Sigma}^0$ and $e^+e^- \rightarrow J/\psi \rightarrow \bar{\Lambda}\Sigma^0$. While currently statistically limited, it provides a novel way to search for possible new sources of CP violation. In the future, the BESIII experiment may provide even higher sensitivity to direct CP violation [35], with further improvement expected from the next generation experiments, e.g., the next-generation tau-charm physics facility [36] and PANDA [37].

ACKNOWLEDGMENTS

The BESIII collaboration thanks the staff of BEPCII and the IHEP computing center for their strong support. This work is supported in part by National Key R&D Program of China under Contracts Nos. 2020YFA0406300, 2020YFA0406400; National Natural Science Foundation of China (NSFC) under Contracts Nos. 11635010, 11735014, 11835012, 11875115, 11935015, 11935016, 11935018, 11961141012, 12022510, 12025502, 12035009, 12035013, 12075250, 12165022, 12192260, 12192261, 12192262, 12192263, 12192264, 12192265, 12225509;

the Chinese Academy of Sciences (CAS) Large-Scale Scientific Facility Program; Joint Large-Scale Scientific Facility Funds of the NSFC and CAS under Contract No. U1832207; the CAS Center for Excellence in Particle Physics (CCEPP); 100 Talents Program of CAS; The Institute of Nuclear and Particle Physics (INPAC) and Shanghai Key Laboratory for Particle Physics and Cosmology; ERC under Contract No. 758462; European Union's Horizon 2020 research and innovation programme under Marie Skłodowska-Curie grant agreement under Contract No. 894790; German Research Foundation DFG under Contracts Nos. 443159800, 455635585, Collaborative Research Center CRC 1044, FOR5327, GRK 2149; Istituto Nazionale di Fisica Nucleare, Italy; Ministry of Development of Turkey under Contract No. DPT2006K-120470; National Science and Technology fund; National Science Research and Innovation Fund (NSRF) via the Program Management Unit for Human Resources & Institutional Development, Research and Innovation under Contract No. B16F640076; Olle Engkvist Foundation under Contract No. 200-0605; STFC (United Kingdom); Suranaree University of Technology (SUT), Thailand Science Research and Innovation (TSRI), and National Science Research and Innovation Fund (NSRF) under Contract No. 160355; Polish National Science Centre under Contract 2019/35/O/ST2/02907; The Royal Society, UK under Contracts Nos. DH140054, DH160214; The Swedish Research Council; U. S. Department of Energy under Contract No. DE-FG02-05ER41374.

Appendix A

1. Monte Carlo simulation

The optimization of the event selection criteria and the estimation of physics background as well as the determination of efficiency are performed using MC simulated samples. The GEANT4-based [38] MC package includes the geometric description of the BESIII detector and the detector response. The inclusive MC sample includes both the production of the J/ψ resonance and the continuum processes incorporated in KKMC [39]. All particle decays are modelled with EVTGEN [40] using branching fractions either taken from the Particle Data Group (PDG) [41], when available, or otherwise estimated with LUNDCHARM [42]. For the signal $J/\psi \rightarrow \bar{\Lambda}\Sigma^0 + c.c.$, the MC samples

are produced using the angular distribution formula shown in Appendix A 6. For the determination of the cross section, the generator CONEXC [43] was used. For the background channels $J/\psi \rightarrow \Sigma\bar{\Sigma}^0$, $J/\psi \rightarrow \Lambda\bar{\Lambda}$, the exclusive MC samples were generated in accordance with their decay amplitudes [11, 44].

2. Initial Selection Criteria

Candidates for $J/\psi \rightarrow \bar{\Lambda}(\rightarrow \bar{p}\pi^+)\Sigma^0(\rightarrow \gamma\Lambda \rightarrow \gamma p\pi^-)$ are required to have four charged tracks with net zero charge and at least one photon.

Charged tracks are selected in the MDC within ± 20 cm of the interaction point in the beam direction and within 10 cm in the plane perpendicular to the beam. The polar angles of these tracks are required to be within the MDC fiducial volume, $|\cos\theta| < 0.93$, where θ is defined with respect to the z -axis, which is the symmetry axis of the MDC. No particle identification is performed to maintain high efficiency.

To reconstruct the decays $\Lambda \rightarrow p\pi^-$ and $\bar{\Lambda} \rightarrow \bar{p}\pi^+$, we loop over all the combinations of positive and negative charged track pairs and require that at least one $(p\pi^-)(\bar{p}\pi^+)$ track hypothesis successfully passes the vertex finding algorithm [45] of Λ and $\bar{\Lambda}$. If more than one accepted combination satisfies the vertex fit requirement, the one with the minimum value of $\sqrt{(M_{p\pi^-} - M_\Lambda)^2 + (M_{\bar{p}\pi^+} - M_\Lambda)^2}$ is chosen, where $M_{p\pi^-}$ ($M_{\bar{p}\pi^+}$) is the $p\pi^-$ ($\bar{p}\pi^+$) invariant mass and M_Λ is the nominal Λ mass [41].

For good photon selection, showers in the EMC identified as photon candidates are required to satisfy fiducial and shower-quality requirements. For the barrel region, showers must have a minimum energy deposition of 25 MeV with the polar angle of each track satisfying $|\cos\theta| < 0.80$, while those from the end cap region must have at least 50 MeV and the polar angle is required to be $0.86 < |\cos\theta| < 0.92$. To remove the noise unrelated with the event, the difference between the EMC time and the event start time (TDC) has to fulfill $0 \leq \text{TDC} \leq 700$ ns. To suppress showers generated by charged particles, the photon candidate angular separation from the nearest charged track is required to be at least 10° .

The selected events are subjected to a four-constraint energy momentum conservation kinematic fit (4C fit) with the hypothesis of $\gamma\Lambda\bar{\Lambda}$. The kinematic fit adjusts the reconstructed particle energy and momentum within the measured errors so as to satisfy energy and momentum conservation for the giv-

an event hypothesis. This improves resolution and reduces background. When there are multiple photon candidates in an event, the combination with the smallest χ_{4C}^2 is retained. The kinematic fit is very powerful to suppress background events with multiple photon candidates in the final states, e.g., $J/\psi \rightarrow \Sigma^0 \bar{\Sigma}^0$ and $J/\psi \rightarrow \Lambda \bar{\Sigma}^0 \pi^0$.

3. Final Selection Criteria

After the initial selection, the scatter plot of $M_{p\pi^-}$ versus $M_{\bar{p}\pi^+}$ of the accepted candidates is shown in Fig. 2, where the clear cluster corresponds to the decays of $\Lambda \rightarrow p\pi^-$ and $\bar{\Lambda} \rightarrow \bar{p}\pi^+$. The Λ and $\bar{\Lambda}$ signal candidates are selected by requiring $|M_{p\pi^-} - M_\Lambda| < 5 \text{ MeV}/c^2$ and $|M_{\bar{p}\pi^+} - M_{\bar{\Lambda}}| < 5 \text{ MeV}/c^2$. To further suppress backgrounds and improve the mass resolution, the 4C kinematic fit must satisfy $\chi_{4C}^2 < 30$. In addition, $M_{\gamma\bar{\Lambda}} > 1.135 \text{ GeV}/c^2$ and $M_{\gamma\Lambda} > 1.135 \text{ GeV}/c^2$ are required in the further analysis for $J/\psi \rightarrow \bar{\Lambda}\Sigma^0$ and $J/\psi \rightarrow \Lambda\bar{\Sigma}^0$, respectively, which has a pronounced effect on suppressing the background events from $J/\psi \rightarrow \Lambda\bar{\Lambda}$. After applying the above requirements, the invariant mass spectrum of $\gamma\Lambda$ ($\gamma\bar{\Lambda}$) is shown in Fig. 3, where the prominent peak of Σ^0 ($\bar{\Sigma}^0$) is clearly observed.

4. Background Analysis

Possible background sources are investigated with an inclusive MC sample of 10 billion J/ψ decays. Using the same selection criteria, with the help of a generic event type analysis tool [46], the surviving background events mainly originate from $J/\psi \rightarrow \Sigma^0 \bar{\Sigma}^0$, $J/\psi \rightarrow \Lambda\bar{\Lambda}$ and $J/\psi \rightarrow \gamma\Lambda\bar{\Lambda}$ (including a resonant contribution from $\gamma\eta_c$), but none of these produce an evident peak in the Σ^0 mass region. The exclusive MC samples of these background channels are generated with the corresponding helicity amplitudes and their contributions are shown in Fig. 3. To estimate the number of background events coming directly from the e^+e^- annihilation, the same analysis is performed on data taken at $\sqrt{s} = 3.080 \text{ GeV}$, where the number of background events, 39 ± 7 is also extracted by fitting the $\gamma\Lambda$ (or $\gamma\bar{\Lambda}$) mass spectrum as shown in Fig. 4. The background events are then normalized to the J/ψ data after taking into account the luminosities and energy-dependent cross sections of continuum processes [47], with the scaling factor

calculated as

$$f = \frac{\mathcal{L}_{J/\psi}}{\mathcal{L}_{\psi(3080)}} \times \frac{s_{\psi(3080)}^5}{s_{J/\psi}^5} \times \frac{\epsilon_{\psi(3080)}}{\epsilon_{J/\psi}}. \quad (\text{A1})$$

Here, \mathcal{L} , s , and ϵ are the integrated luminosity, the square of the centre-of-mass energy, and the detection efficiency at the two c.m. energies, respectively. the number of background events for $J/\psi \rightarrow \bar{\Lambda}\Sigma^0$ is normalized to be 669 ± 120 . It should be pointed out that there is no interference between the QED background and the J/ψ resonance since this is a purely electromagnetic process according to Ref. [23].

5. Signal Extraction

The signal yields are obtained from an extended unbinned maximum likelihood fit to the $\gamma\Lambda$ ($\gamma\bar{\Lambda}$) mass spectrum. The total probability density function (PDF) consists of a signal and various background contributions. The signal component is modeled as the MC simulated signal shape convolved with a Gaussian function to account for the difference in the mass resolution between data and MC simulation. The background components, $J/\psi \rightarrow \Sigma^0 \bar{\Sigma}^0$, $J/\psi \rightarrow \Lambda\bar{\Lambda}$, and $J/\psi \rightarrow \gamma\Lambda\bar{\Lambda}$ ($\gamma\eta_c$), as well as the reflection from signal conjugation decay mode, are described with the simulated shapes derived from the dedicated MC samples, while the magnitudes of different components are left free to account for the uncertainties of the branching fractions of these decays and other intermediate decays. The fit to the $M_{\gamma\Lambda}/M_{\gamma\bar{\Lambda}}$ spectrum, as displayed in Fig. 3, gives $26260 \pm 181 \bar{\Lambda}\Sigma^0$ events.

6. Helicity Amplitude

The structure of the six dimensional angular distribution is determined by global parameters $\omega = (\alpha_{J/\psi}, \Delta\Phi, \alpha_\gamma, \alpha_\Lambda, \alpha_{\bar{\Lambda}})$ independent of the Σ^0 scattering angle, θ_{Σ^0} , and is written in a modular form as

$$\mathcal{W}(\xi; \omega) = \sum_{\mu, \nu=0}^3 \sum_{\mu', \nu'=0}^3 C_{\mu\nu} a_{\mu\mu'}^{\Sigma^0} a_{\mu'\nu'}^{\Lambda} a_{\nu\nu'}^{\bar{\Lambda}}, \quad (\text{A2})$$

where the $C_{\mu\nu}(\theta; \alpha_{J/\psi}, \Delta\Phi)$ is a 4×4 spin density matrix, describing the spin configuration of the entangled hyperon-antihyperon pair. The matrix elements

are expressed as

$$C_{\mu\nu} = (1 + \alpha_{J/\psi} \cos^2 \theta) \begin{pmatrix} 1 & 0 & P_y & 0 \\ 0 & C_{xx} & 0 & C_{xz} \\ -P_y & 0 & C_{yy} & 0 \\ 0 & -C_{xz} & 0 & C_{zz} \end{pmatrix}, \quad (\text{A3})$$

where P_y governs the polarization of the Σ^0 and C_{ij} characterizes its spin correlations. Both P_y and C_{ij} can be written in terms of $\sin \Delta\Phi$ or $\cos \Delta\Phi$ as

$$P_y = f(\theta) \sin \Delta\Phi, C_{xz} = f(\theta) \cos \Delta\Phi, \quad (\text{A4})$$

where $f(\theta)$, a common function dependent on the Σ^0 ($\bar{\Sigma}^0$) direction angle θ , is expressed as

$$f(\theta) = \frac{\sqrt{1 - \alpha_{J/\psi}^2} \sin \theta \cos \theta}{1 + \alpha_{J/\psi} \cos^2 \theta}. \quad (\text{A5})$$

The matrices $a_{\mu\nu}^Y$ in Eq. (A2) represent the propagation of the spin density matrices in the sequential decays. The full expressions of $C_{\mu\nu}$ and $a_{\mu\nu}^Y$ are given in Ref. [48].

7. Global Fit of Parameters

A non-zero phase angle difference $\Delta\Phi$ indicates the transverse hyperon polarization, which allows us to measure these parameters at the same time. A simultaneous fit is performed to the two conjugate channels, $J/\psi \rightarrow \bar{\Lambda}\Sigma^0$ and $J/\psi \rightarrow \Lambda\bar{\Sigma}^0$. The likelihood function constructed from the probability density function for an event characterized by ξ_i is

$$\mathcal{L} = \prod_{i=1}^N \mathcal{P}(\xi_i; \omega) = \prod_{i=1}^N \frac{\mathcal{W}(\xi_i; \omega) \epsilon(\xi_i)}{\mathcal{N}(\omega)}, \quad (\text{A6})$$

where $\epsilon(\xi_i)$ is the detection efficiency, N is the number of the surviving data events after all selection criteria, the normalization factor $\mathcal{N}(\omega) = \int \mathcal{W}(\xi; \omega) \epsilon(\xi) d\xi$, with $\mathcal{W}(\xi; \omega)$ defined in Eq. (A2), and \mathcal{P} is the probability to produce event i based on the measured parameters ξ_i and the set of observables ω . Based on the likelihood function defined in Eq. (A6), the objective function is written as

$$S = -\ln \mathcal{L}_{\text{data}}^{\text{I}} - \ln \mathcal{L}_{\text{data}}^{\text{II}} + \ln \mathcal{L}_{\text{bkg}}^{\text{I}} + \ln \mathcal{L}_{\text{bkg}}^{\text{II}}, \quad (\text{A7})$$

where $\ln \mathcal{L}_{\text{data}}^{\text{I,II}}$ and $\ln \mathcal{L}_{\text{bkg}}^{\text{I,II}}$ are the likelihood functions for $J/\psi \rightarrow \bar{\Lambda}\Sigma^0$ and $J/\psi \rightarrow \Lambda\bar{\Sigma}^0$ and the background

events from simulation, respectively. In order to optimize the free parameters ($\alpha_{J/\psi}$, $\Delta\Phi_1$ and $\Delta\Phi_2$) and minimize the objective function, the normalization factor $\mathcal{N}(\omega)$ in Eq. (A6) is obtained by MC integral generated by phase space through all event selection criteria. To compare the fit with data, the moments directly related to helicity amplitude are defined as:

$$\begin{aligned} T_1 &= \sum_i^{N_k} \left(\cos^2 \theta n_{1,z}^{(i)} n_{2,z}^{(i)} - \sin^2 \theta n_{1,x}^{(i)} n_{2,x}^{(i)} \right), \\ T_2 &= \sum_i^{N_k} \cos \theta \sin \theta \left(n_{1,z}^{(i)} n_{2,x}^{(i)} - n_{1,x}^{(i)} n_{2,z}^{(i)} \right), \\ T_3 &= \sum_i^{N_k} \cos \theta \sin \theta n_{1,y}^{(i)}, \\ T_4 &= \sum_i^{N_k} \cos \theta \sin \theta n_{2,y}^{(i)}, \\ T_5 &= \sum_i^{N_k} \left(n_{1,z}^{(i)} n_{2,z}^{(i)} - \sin^2 \theta n_{1,y}^{(i)} n_{2,y}^{(i)} \right), \end{aligned} \quad (\text{A8})$$

where N_k is the number of events in the k^{th} $\cos \theta$ bin and $\hat{\mathbf{n}}_1$ ($\hat{\mathbf{n}}_2$) is the unit vector in the direction of the nucleon (anti-nucleon) in the rest frame of Σ^0 ($\bar{\Lambda}$) for $J/\psi \rightarrow \bar{\Lambda}\Sigma^0$, as illustrated in Fig. 5. The resulting T_i distributions for data and the fit results are shown in Figs. 6 and 7, and the difference between T_3 and T_4 results from the transverse polarization of Σ^0 ($\bar{\Sigma}^0$), which allows the relative phase between G_E and G_M to be determined from the global fit of polarization with the modulus of the ratio between G_E and G_M obtained from $\alpha = \frac{s-4M_Y^2 R^2}{s+4M_Y^2 R^2}$.

8. Systematic Uncertainty

The uncertainties in the measurement of the form factors are mainly from the $\Lambda, \bar{\Lambda}$ reconstruction, the 4C kinematic fit, and the background estimation. For the $\Lambda, \bar{\Lambda}$ reconstruction, a correction to the MC efficiency is made. We also use the control sample of $J/\psi \rightarrow \bar{p}K^+\Lambda$ to obtain the efficiencies of the data and MC simulation in the Λ and $\bar{\Lambda}$ reconstruction, and then correct the MC efficiencies by the observed data-MC efficiency differences. In order to reduce the impact of statistical fluctuations, the fit with the corrected MC sample is performed 400 times by varying the correction factor randomly within one standard deviation. The differences between the results with

and without correction are taken as the systematic uncertainties. For the 4C kinematic fit, the MC sample in the polarization fit is altered by changing the helix parameters of charged tracks, and the same fit procedure is performed to the same data sample. The relative differences of the fit results are assigned as the uncertainties. The systematic uncertainty arising from the background estimate for each background source is assigned by varying the normalization factor by one standard deviation, the maximum change of the result is assigned as the associated systematic uncertainty. The total systematic uncertainty due to the background estimate is obtained by adding all effects of various background sources in quadrature. The uncertainties due to the $\alpha_{\Lambda, \bar{\Lambda}}$ are estimated by varying the quoted value from Ref. [33] within one standard deviation. The systematic uncertainties for the polarization measurement, as discussed above, are

listed in Table I.

TABLE I. Relative systematic uncertainties for the parameters measurement (%).

Source	$\alpha_{J/\psi}$	$\Delta\Phi_1$	$\Delta\Phi_2$
$\Lambda/\bar{\Lambda}$ reconstruction	1.13	0.38	0.17
Kinematic fit	0.24	0.40	0.23
Background estimate	1.99	0.64	0.33
$\alpha_{\Lambda/\bar{\Lambda}}$	0.00	0.49	0.09
Total	2.30	0.98	0.45

- [1] R. W. McAllister and R. Hofstadter, *Phys. Rev.* **102**, 851 (1956).
- [2] V. Punjabi, C. F. Perdrisat, M. K. Jones, E. J. Brash and C. E. Carlson, *Eur. Phys. J. A* **51**, 79 (1956).
- [3] A. J. R. Puckett *et al.* (Jefferson Lab Hall A Collaboration), *Phys. Rev. C* **85**, 045203 (2012).
- [4] M. Ablikim *et al.* (BESIII Collaboration), *Phys. Lett. B* **817**, 136328 (2021).
- [5] Y. H. Lin, H. W. Hammer and U. Meißner, *Phys. Lett. B* **816**, 136254 (2021).
- [6] A. Mangoni, S. Pacetti, and E. Tomasi-Gustafsson, *Phys. Rev. D* **104**, 116016 (2021).
- [7] J. Segovia, I. C. Cloet, C. D. Roberts, and S. M. Schmidt, *Few Body Syst.* **55**, 1185 (2014).
- [8] M. Ablikim *et al.* (BESIII Collaboration), *Nuovo Cim. C* **40**, 28 (2017).
- [9] M. Ablikim *et al.* (BESIII Collaboration), *PoS BORMIO2017*, 004 (2017).
- [10] M. Ablikim *et al.* (BESIII Collaboration), *EPJ Web Conf* **192**, 00023 (2018).
- [11] M. Ablikim *et al.* (BESIII Collaboration), *Nature Phys.* **15**, 631 (2019).
- [12] M. Ablikim *et al.* (BESIII Collaboration), *PoS ICHEP2018*, 550 (2019).
- [13] M. Ablikim *et al.* (BESIII Collaboration), *EPJ Web Conf.* **199**, 03009 (2019).
- [14] M. Ablikim *et al.* (BESIII Collaboration), *PoS SPIN2018*, 121 (2019).
- [15] M. Ablikim *et al.* (BESIII Collaboration), *J. Phys. Conf. Ser.* **1137**, 012010 (2019).
- [16] M. Ablikim *et al.* (BESIII Collaboration), *Nuovo Cim. C* **42**, 111 (2019).
- [17] M. Ablikim *et al.* (BESIII Collaboration), *AIP Conf. Proc.* **2130**, 040009 (2019).
- [18] M. Ablikim *et al.* (BESIII Collaboration), *J. Phys. Conf. Ser.* **1435**, 012031 (2020).
- [19] M. Ablikim *et al.* (BESIII Collaboration), *Phys. Lett. B* **814**, 136110 (2021).
- [20] M. Ablikim *et al.* (BESIII Collaboration), *Phys. Lett. B* **831**, 137187 (2022).
- [21] M. Ablikim *et al.* (BESIII Collaboration), *Phys. Rev. D* **106**, L091101 (2022).
- [22] M. Ablikim *et al.* (BESIII Collaboration), *Phys. Rev. Lett.* **123**, 122003 (2019).
- [23] R. B. Ferroli, A. Mangoni, and S. Pacetti, *Eur. Phys. J. C* **80**, 903 (2020).
- [24] E. Perotti, *Ph.D. thesis, Uppsala U.* (2020).
- [25] M. Ablikim *et al.* (BESIII Collaboration), *Chin. Phys. C* **46**, 074001 (2022).
- [26] M. Ablikim *et al.* (BESIII Collaboration), *Nucl. Instrum. Meth. A* **614**, 345 (2010).
- [27] C. H. Yu *et al.*, *Proceedings of IPAC2016, Busan, Korea, 2016*, doi:10.18429/JACoW-IPAC2016-TUYA01.
- [28] M. Ablikim *et al.* (BESIII Collaboration), *Phys. Lett. B* **791**, 375 (2019).
- [29] A. Z. Dubnickova, S. Dubnička, and M. P. Rekaló, *Nuovo Cimento A* **109**, 241 (1996).
- [30] S. Pacetti, R. B. Ferroli, and E. Tomasi-Gustafsson, *Phys. Rep.* **550**, 1 (2015).
- [31] G. Fäldt, and A. Kupsc, *Phys. Lett. B* **772**, 16 (2017).
- [32] J. Haidenbauer, U. Meißner, and L. Y. Dai, *Phys. Rev. D* **103**, 014028 (2021).

- [33] M. Ablikim *et al.* (BESIII Collaboration), *Phys. Rev. Lett.* **129**, 131801 (2022).
- [34] G. Fäldt, *Phys. Rev. D* **97**, 053002 (2018).
- [35] M. Ablikim *et al.* (BESIII Collaboration), *Chin. Phys. C* **44**, 040001 (2022).
- [36] N. Salone, P. Adlarson, V. Batozskaya, S. Leupold, and J. Tandean, *Phys. Rev. D* **105**, 116022 (2022).
- [37] G Barucca *et al.*, *Eur. Phys. J. A* **57**, 154 (2021).
- [38] S. Agostinelli *et al.*, *Nucl. Instrum. Meth. A* **506**, 250 (2003).
- [39] S. Jadach, B. F. L. Ward, and Z. Was, *Phys. Rev. D* **63**, 113009 (2001); *Comput. Phys. Commun.* **130**, 260 (2000).
- [40] D. J. Lange, *Nucl. Instrum. Meth. A* **462**, 152 (2001); R. G. Ping, *Chin. Phys. C* **32**, 599 (2008).
- [41] P. A. Zyla *et al.*, *Prog. Theor. Exp. Phys.* **2022**, 083C01 (2022).
- [42] J. C. Chen, G. S. Huang, X. R. Qi, D. H. Zhang, and Y. S. Zhu, *Phys. Rev. D* **62**, 034003 (2000); R. L. Yang, R. G. Ping, and H. Chen, *Chin. Phys. Lett.* **31**, 061301 (2014).
- [43] R. G. Ping, *Chin. Phys. C* **38**, 083001 (2014).
- [44] B. Zhong, R. G. Ping, and Z. J. Xiao, *Chin. Phys. C* **32**, 692 (2008).
- [45] M. Xu *et al.*, *Chin. Phys. C* **33**, 428 (2009).
- [46] X. Y. Zhou, S. X. Du, G. Li, and C. P. Shen, *Comput. Phys. Commun.* **258**, 107540 (2021).
- [47] S. J. Brodsky and G. R. Farrar, *Phys. Rev. Lett.* **31**, 1153 (1973).
- [48] E. Perotti, G. Fäldt, A. Kupsc, S. Leupold, and J. J. Song, *Phys. Rev. D* **99**, 056008 (2019).